Temperature Dependence of Dynamics and Thermodynamics of the Regulatory Domain of Human Cardiac Troponin C†

Leo Spyracopoulos,*,‡ Pierre Lavigne,§ Matthew P. Crump,|| Stéphane M. Gagné,⊥ Cyril M. Kay,‡,# and Brian D. Sykes#,@

Department of Biochemistry, The Protein Engineering Network of Centers of Excellence, CIHR Group in Protein Structure and Function, and National High Field Nuclear Magnetic Resonance Center, University of Alberta, Edmonton, Alberta, T6G 2H7 Canada, Université de Sherbrooke, Sherbrooke, Québec, J1K 2R1 Canada, University of Southampton, Highfield, Southhampton, SO17 1BJ U.K., and Université Laval, Québec, G1K 7P4 Canada

Received May 2, 2001; Revised Manuscript Received August 13, 2001

ABSTRACT: Binding of Ca^{2+} to the regulatory domain of troponin C (TnC) in cardiac muscle initiates a series of protein conformational changes and modified protein−protein interactions that initiate contraction. Cardiac TnC contains two Ca^{2+} binding sites, with one site being naturally defunct. Previously, binding of Ca^{2+} to the functional site in the regulatory domain of TnC was shown to lead to a decrease in conformational entropy ($T\Delta S$) of 2 and 0.5 kcal mol^{-1} for the functional and nonfunctional sites, respectively, using ^{15}N nuclear magnetic resonance (NMR) relaxation studies [Spyracopoulos, L., et al. (1998) *Biochemistry 37*, 18032−18044]. In this study, backbone dynamics of the Ca^{2+}-free regulatory domain are investigated by backbone amide ^{15}N relaxation measurements at eight temperatures from 5 to 45 °C. Analysis of the relaxation measurements yields an order parameter (S^2) indicating the degree of spatial restriction for a backbone amide H−N vector. The temperature dependence of S^2 allows estimation of the contribution to protein heat capacity from pico- to nanosecond time scale conformational fluctuations on a per residue basis. The average heat capacity contribution ($C_{p,j}$) from backbone conformational fluctuations for regions of secondary structure for the regulatory domain of cardiac apo-TnC is 6 cal mol^{-1} K^{-1}. The average heat capacity for Ca^{2+} binding site 1 is larger than that for site 2 by 1.3 ± 0.8 cal mol^{-1} K^{-1}, and likely represents a mechanism where differences in affinity between Ca^{2+} binding sites for EF hand proteins can be modulated.

Contraction of cardiac and skeletal striated muscle commences with Ca^{2+} binding to the regulatory domain of the thin filament protein TnC.[1] This Ca^{2+} binding event is conveyed through the thin filament by a series of structural changes and modified protein−protein interactions, exposing binding sites for myosin on the actin filament. Following binding of myosin heads to the actin thin filament, the power stroke is ultimately responsible for muscle contraction (for reviews, see refs *1*−*3*). In cardiac and skeletal muscle, TnC is a largely α-helical protein with a mass of ∼18 kDa. TnC consists of two domains, similar in size and joined by a flexible linker, with two Ca^{2+} binding sites per domain (*4*−*6*). The Ca^{2+} binding sites are dubbed EF hand helix−loop−helix motifs. The C-terminal domain contains Ca^{2+} binding sites 3 and 4, and the N-terminal domain contains sites 1 and 2. Sites 3 and 4 are always filled with Ca^{2+} or Mg^{2+} in intact muscle, and thus, the C-domain is termed the "structural" domain. The N-terminal domain is termed the "regulatory" domain with weaker Ca^{2+} affinity in the range of physiological changes. Due to sequence differences (*7*) in Ca^{2+} binding sites, the regulatory domain in cardiac TnC binds only a single Ca^{2+} in site 2, whereas the regulatory domain of skeletal TnC binds two Ca^{2+} ions, one in site 1 and one in site 2 (*8*).

Ca^{2+} binding to the regulatory domain of sTnC leads to extensive shifts of helices that result in a structural "opening" concurrent with the display of a hydrophobic surface (*4*, *5*, *9*−*11*). The exposed hydrophobic surface is the recognition site for resultant protein−protein interactions in the troponin complex that lead to muscle contraction. Different from the case for sTnC, large structural changes do not occur when Ca^{2+} binds site 2 in cNTnC, due in large part to the inability of site 1 to bind Ca^{2+} (*12*, *13*). However, $1Ca^{2+}$•cNTnC has recently been shown to experience a structural opening analogous to that for sNTnC in the presence of its target cardiac troponin I peptide (*14*). Thus, while $2Ca^{2+}$•sNTnC and $1Ca^{2+}$•cNTnC bind their respective peptides in essentially the same conformational state, the thermodynamic and kinetic equilibria for the two systems are different, contributing in part to physiological differences between the two muscle types (*15*).

Relaxation of backbone amide ^{15}N nuclei provides details of the rotational tumbling and internal dynamics of proteins (*16*−*18*). The Lipari−Szabo model-independent formalism is typically used to analyze relaxation data of proteins, and

† This work was supported by the Canadian Institutes of Health Research (CIHR) and the Heart and Stroke Foundation of Canada.

* To whom correspondence should be addressed. E-mail: leo.spyracopoulos@ualberta.ca. Phone: (780) 492-2417. Fax: (780) 492-0886.

‡ Department of Biochemistry, University of Alberta.

§ Université de Sherbrooke.

|| University of Southampton.

⊥ Université Laval.

The Protein Engineering Network of Centers of Excellence, University of Alberta.

@ CIHR Group in Protein Structure and Function, and National High Field Nuclear Magnetic Resonance Center, University of Alberta.

[1] Abbreviations: CD, circular dichroism; N- and CTnC, N- and C-terminal domains of troponin C, respectively; s- and cTnC, skeletal and cardiac troponin C, respectively; HSQC, heteronuclear single-quantum coherence; NMR, nuclear magnetic resonance; NOE, nuclear Overhauser effect.

10.1021/bi010903k CCC: $20.00
Published on Web 09/22/2001

provides an overall rotational correlation time, an internal correlation time, and an order parameter (S^2) for potentially every backbone amide $^{15}N-^{1}H_N$ vector in a protein (*19*−*21*). S^2 is a useful parameter since it can be interpreted in the absence of a specific motional model. With respect to determination of thermodynamic quantities such as enthalpy and conformational entropy, interpretation of S^2 using a diffusion-in-a-cone model for a backbone amide $^{15}N-^{1}H_N$ vector within a polypeptide is fairly robust for semiquantitative calculations (*22*−*25*). It is important to note, however, that interpretation of thermodynamic quantities estimated from S^2 values derived from NMR relaxation data is hampered due to the fact that effects of correlated motion between different molecular segments are difficult to assess. Additionally, it is not clear if partitioning of NMR observable and nonobservable motions in the calculation of entropy is valid. At present, if the entropy determined using NMR relaxation measurements for different backbone amide sites within a protein is summed, the result is best viewed as an upper limit to the total entropy contributed from backbone conformational fluctuations on the pico- to nanosecond time scale. Notably, particular caution must be exercised when estimating thermodynamic changes for unfolding transitions when summing per residue changes based on backbone amide ^{15}N relaxation measurements (*26*).

Recently, we have determined that the backbone conformational entropy difference between sites 1 and 2 of Ca^{2+}-free sNTnC is at most 1 kcal mol^{-1} K^{-1}, determined from pico- to nanosecond time scale bond vector oscillations that give rise to backbone amide ^{15}N NMR relaxation (*27*). The conformational entropy difference between sites 1 and 2 of apo-sNTnC is similar to the difference in free energy of Ca^{2+} binding between the sites and consistent with the hypothesis that site 2 binds Ca^{2+} prior to site 1 by virtue of its greater rigidity. Unfortunately, changes in backbone conformational entropy induced by Ca^{2+} binding to sNTnC have not been measured via NMR relaxation due to complications related to dimerization of $2Ca^{2+}$·sNTnC. For apo-cNTnC, the backbone of site 2 is similar in flexibility to apo-sNTnC, whereas for site 1, it is more rigid than in apo-sNTnC (*28*). The greater rigidity for the backbone of site 1 in apo-cNTnC is due in part to sequence differences between the two isoforms that include substitution of hydrophobic residues for acidic residues in site 1 of cNTnC. Ca^{2+} binding to site 2 of cNTnC decreases the backbone conformational entropy or $T\Delta S$ (decreases flexibility) by at most 2.2 kcal mol^{-1}, as determined by measurements of ^{15}N NMR relaxation (*28*). While site 1 is naturally defunct in the cardiac isoform, Ca^{2+} binding to site 2 decreases the flexibility in site 1, indicating that the Ca^{2+} binding sites are structurally and dynamically coupled.

In this study, the temperature dependence of the backbone dynamics of apo-cNTnC is probed by measurements of backbone amide ^{15}N relaxation at 5, 15, 25, 30, 33, 35, 40, and 45 °C, and at a magnetic field strength of 11.7 T (or a ^{1}H Larmor frequency of ∼500 MHz). Analysis of the temperature dependence of backbone amide $^{15}N-^{1}H_N$ S^2 values is useful for estimating the contribution to protein entropy and heat capacity from pico- to nanosecond time scale conformational fluctuations (*25*). The heat capacity is related to the conformational energy landscape that is sampled by a given backbone amide $^{15}N-^{1}H_N$ vector within a protein. Thus, determination of the temperature dependence of protein flexibility via NMR relaxation measurements can yield important insights into the biological function of a protein. Additionally, temperature-dependent ^{15}N NMR relaxation measurements are also important for probing activation energies of phenomenological slow time scale (micro- to millisecond) motions (*29*).

MATERIALS AND METHODS

Sample Preparation. The expression vector for cNTnC (residues 1−89) was engineered as described previously (*30*). The ^{15}N-labeled protein was expressed in *Escherichia coli* as previously described (*31*, *32*). Purification of the protein was achieved using previously described protocols employed for cleaved sTnC (*33*). cNTnC was obtained in the apo state as previously described for sNTnC (*31*). NMR samples contained 500 μL of a 9:1 H_2O/D_2O mixture (pH 6.7), 100 mM KCl, 15 mM DTT, 15 mM EDTA, ∼2 mM protein for apo-cNTnC, and 0.03% NaN_3.

NMR Spectroscopy. NMR spectra were acquired using a Varian Unity INOVA 500 MHz spectrometer equipped with a 5 mm triple-resonance probe and *z*-axis pulsed field gradients. ^{15}N-T_1, ^{15}N-T_2, and $\{^{1}H\}-^{15}N$ NOE experiments were conducted at 5, 15, 25, 30, 33, 35, 40, and 45 °C using enhanced sensitivity, gradient pulse sequences developed by Farrow et al. (*34*) at 500 MHz. ^{15}N-T_1 data were acquired once at all temperatures using relaxation delays of 11.1, 55.5, 122.1, 199.8, 277.5, 388.5, 499.5, 666.0, 888.0, and 1254.3 ms. ^{15}N-T_2 data were acquired once at each temperature using delays of 16.6, 33.2, 49.8, 66.4, 83.0, 99.7, 116.3, 132.9, 149.5, and 166.1 ms. For the T_1 pulse sequence, the delay between transients was 1.5 s at 5, 15, 25, 30, 35, and 40 °C, 1.0 s at 33 °C, and 2.5 s at 45 °C. For the T_2 pulse sequence, the delay between transients was 3.5 s at 5 and 15 °C and 3 s at 25, 30, 33, 35, 40, and 45 °C. Long recycle delays for the T_2 pulse sequence reduce effects of sample heating due to the electric component of the applied radio frequency fields during the Carr−Purcell−Meiboom−Gill pulse train, as previously noted (*27*). $\{^{1}H\}-^{15}N$ NOEs were measured by recording spectra in the presence and absence of proton saturation. The spectrum recorded without proton saturation was acquired with a delay between transients of 5 s. The spectrum recorded in the presence of proton saturation incorporated a relaxation delay of 2 s, followed by a 3 s proton saturation for a total delay between transients of 5 s.

Thermal Denaturation Monitored by Circular Dichroism Spectroscopy. Temperature denaturation of apo-cNTnC was followed by measurement of CD spectra. Spectra were collected with constant N_2 flushing on a Jasco J-500C spectropolarimeter fitted with a Jasco DP-500N data processor (Jasco, Easton, MD). The temperature of the cell was controlled by a Lauda water bath (model RMS, Brinkmann Instruments, Rexdale, ON). Routine calibration of the instrument was performed with an aqueous solution of *d*-10-(+)-camphorsulfonic acid at 290.5 nm. Ellipticity is given as mean residue ellipticity ($[\theta]$) in degrees per square centimeter per decimole. Mean residue ellipticity was calculated with the equation $[\theta] = [\theta]_{obs}(mrw)/(10lc)$, where $[\theta]_{obs}$ is the ellipticity measured in degrees, mrw is the mean residue weight (molecular mass divided by the number of amino acid residues), c is the protein concentration in grams

per milliliter, and l is the optical path length of the cell in centimeters. The mean residue ellipticity at 222 nm was fit using the program xcrvfit (executable available at http://www.pence.ualberta.ca) assuming a two-state unfolding reaction as previously described (*35*).

Data Processing and Analysis. All spectral processing was accomplished with the program NMRPipe (*36*). Sorting and processing of the superposed orthogonal components of the sensitivity-enhanced two-dimensional free induction decays was performed with the ranceY.M macro within the NMRPipe software. Postacquisition processing of the t_2 interferograms for removal of residual water was not necessary, as previously noted (*27*). For apo-cNTnC, 60°-shifted sine and sine-squared window functions were applied in t_2 and t_1, respectively, at 5 and 15 °C, 60°-shifted sine and 75°-shifted sine-squared windows were applied in t_2 and t_1, respectively, at 25 °C, and 75°-shifted sine and 75°-shifted sine-squared windows were applied in t_2 and t_1, respectively, at 30, 33, 35, 40, and 45 °C. A total of 48 complex points were collected in the t_1 domain for all temperatures. The t_1 domain was extended by half the number of experimental points with linear prediction at 5, 15, and 25 °C, and one-third the number of experimental points at 30, 33, 35, 40, and 45 °C. The t_2 and t_1 domains were extended to twice the number of points with zero filling. Baseline correction was performed with an automatic polynomial subtraction in the F_2 dimension, and the region upfield of 6.5 ppm was discarded. The two-dimensional (2D) $\{^1H-^{15}N\}$-HSQC NMR spectrum containing the most intense resonances in a given T_1 or T_2 decay series or the $\{^1H\}-^{15}N$ NOE spectrum obtained without proton saturation was peak-picked manually with the PIPP program (*37*). All remaining peak intensities were picked automatically with the program CAPP (*37*). The entire procedure, from sorting of the FIDs to peak peaking, was performed automatically using in-house written UNIX shell scripts. T_1 and T_2 values were obtained by nonlinear least-squares fits of the $^{15}N-^1H_N$ cross-peak intensities to a two-parameter exponential decay using software provided by L. E. Kay. Uncertainties in the measured T_1 and T_2 data were obtained from the nonlinear least-squares fits. Uncertainties in the NOE values were estimated from the base-plane noise in the 2D $\{^1H-^{15}N\}$-HSQC NMR spectra recorded with and without proton saturation.

Analysis of ^{15}N-T_1, ^{15}N-T_2, and $\{^1H\}-^{15}N$ NOE. An in-depth analysis of the temperature dependence of backbone amide motions sensed by ^{15}N NMR relaxation measurements requires reliable values of S^2 to be extracted from relaxation data for apo-cNTnC. The model-independent analysis for apo-cNTnC was carried out under the assumption of isotropic rotational tumbling. For each residue, relaxation data were fit to a motional model describing overall molecular tumbling of the protein, and including one or two types of internal motions with various time scales. As previously described, the basic motional model is separated into five specific models for computational purposes (*34*). Model 1 has an order parameter (S^2) describing the amplitude of spatial restriction for a backbone amide N−NH vector which can vary from 0 (no motional restriction) to 1 (complete motional restriction) and a correlation time for overall molecular reorientation (τ_m). Model 2 has S^2, τ_m, and a correlation time for picosecond time scale internal motions (τ_f). Model 1 assumes that internal motions within the protein are extremely fast and do not contribute to relaxation ($\tau_f \rightarrow 0$), whereas model 2 assumes that internal motions are within the $10^{-10}-10^{-12}$ s time scale ($0 < \tau_f < \tau_m$). Model 3 is model 1, modified to include a parameter describing the rate of microsecond to millisecond time scale internal motions (R_{ex}, in s^{-1}). Model 4 is model 3, modified to include the parameter R_{ex}. Finally, model 5 accounts for internal motions that occur on two time scales (see the Appendix).

Analysis of Thermodynamics for Backbone Fluctuations. Following the work of Akke et al. (*22*), Yang and Kay (*24*) derived an expression from which the entropy associated with picosecond to nanosecond time scale bond vector fluctuations may be calculated in a semiquantitative fashion:

$$\frac{S_{p,j}}{k} = \ln[\pi(3 - \sqrt{1 + 8S})] \quad (1)$$

where k is Boltzmann's constant, $S_{p,j}$ is the entropy change associated with the jth backbone amide $^{15}N-^1H_N$ vector, and S is the square root of the Lipari−Szabo order parameter. From the temperature dependence of S^2, and using eq 1, the heat capacity contribution from picosecond to nanosecond motions of a bond vector can be estimated by (*25*):

$$C_{p,j} = \frac{\partial S_{p,j}(T)}{\partial[\ln(T)]} \quad (2)$$

where $S_{p,j}$ is given in eq 1. It is expected that the entropy, $S_{p,j}$, increases linearly with respect to $\ln(T)$ for the folded state of a protein. Thus, the slope of $S_{p,j}$ as a function of the natural logarithm of the temperature gives the heat capacity, $C_{p,j}$ (eq 2). It should be noted, however, that the slope, $d(1 - \sqrt{S^2})/dT$, derived from plotting $1 - \sqrt{S^2}$ as a function of temperature (*29*) yields essentially identical information as estimates of the heat capacity from eq 2. Interpretation of $d(1 - \sqrt{S^2})/dT$, however, has the advantage that assumptions do not need to be made with respect to the details of the underlying motions governing relaxation of a given $^{15}N-^1H_N$ backbone amide pair. In addition, no assumptions regarding the separability of motions that can and cannot be observed by NMR are required. However, the effect of correlated motion between different backbone segments of a polypeptide on the value of S^2 remains difficult to assess; therefore, interpretation of $d(1 - \sqrt{S^2})/dT$ or heat capacity must be conservative. The problems of correlated motion and separability of motions presently plague semiquantitative calculation and subsequent interpretation of thermodynamic quantities from NMR relaxation data, such as entropy and heat capacity. However, recent results from quasi-harmonic analysis of molecular dynamics simulations indicate that separability of NMR observable and nonobservable motions is a good approximation, and that the effects of correlated motions may not be severe, at least for dominant protein motions on the nanosecond time scale, for the folded state of a protein (*38*). In addition, S^2 values determined for apo-cNTnC using model 5 showed an increase with increasing temperature for the flexible N-terminal residues, and this is not physically reasonable (see the Discussion). Therefore, we have employed the method of Schurr et al. to extract meaningful values of S^2 (*39*). Briefly, the relaxation data are fit to the $S^2-\tau_m-\tau_f$ model on a per residue basis (i.e., we do not assume a single, global τ_m), and distinguished from

parameters determined with the Lipari−Szabo model-independent analysis by using the notation $S'^2-\tau'_m-\tau'_f$. So long as $0.15 \leq S'^2 \leq 1.0$, $0 \leq \tau'_f \leq 300$ ps, and 2 ns $\leq \tau_j \leq$ 15 ns (where τ_j is the *j*th correlation time for a distribution of correlation times), the value of S'^2 extracted in this manner will differ by less than 10% from the true value of S^2 (*25*).

RESULTS

^{15}N-T_1, ^{15}N-T_2, and NOE Data. Backbone amide ^{15}N and ^1H_N chemical shift assignments for apo-cNTnC have been reported previously (*13*). Backbone amide ^{15}N and ^1H_N chemical shift assignments for apo-cNTnC at 5, 15, 25, 30, 33, 35, 40, and 45 °C were accomplished by following temperature-dependent chemical shift changes in 2D {^{1}H−^{15}N}-HSQC NMR spectra. For apo-cNTnC, ^{15}N NMR relaxation data for 65, 71, 73, 63, 60, 67, 68, and 64 of a total of 89 residues were obtained at 5, 15, 25, 30, 33, 35, 40, and 45 °C, respectively. Of the uncharacterized residues at all temperatures, M1 and D2 were not observed, likely due to rapid exchange with water, and prolines 52 and 54 do not have amide protons. The remaining residues were partially or completely overlapped in the 2D {^{1}H−^{15}N}-HSQC NMR spectra, or difficult to assign by following chemical shift changes as a function of temperature and therefore excluded from the present analysis. The average T_1 for all residues was 652 ± 35, 531 ± 18, 457 ± 20, 435 ± 25, 412 ± 20, 410 ± 24, 414 ± 102, and 413 ± 120 ms at 5, 15, 25, 30, 33, 35, 40, and 45 °C, respectively. The average error of the T_1 value was 3, 5, 4, 3, 7, 3, 6, and 5 ms at 5, 15, 25, 30, 33, 35, 40, and 45 °C, respectively. The average T_2 for all residues was 91 ± 51, 107 ± 12, 135 ± 15, 147 ± 16, 153 ± 16, 157 ± 14, 187 ± 83, and 198 ± 84 ms at 5, 15, 25, 30, 33, 35, 40, and 45 °C, respectively. The average error of the T_2 value was 1 ms at 5, 15, 25, 30, and 35 °C and 2, 2, and 3 ms at 33, 40, and 45 °C, respectively. The average NOE for all residues was 0.65 ± 0.23, 0.70 ± 0.10, 0.67 ± 0.01, 0.65 ± 0.11, 0.63 ± 0.11, 0.62 ± 0.11, 0.59 ± 0.23, and 0.56 ± 0.26 at 5, 15, 25, 30, 33, 35, 40, and 45 °C, respectively. The average error of the NOE value was 0.02, 0.01, 0.01, 0.01, 0.03, 0.01, 0.03, and 0.03 at 5, 15, 25, 30, 33, 35, 40, and 45 °C, respectively. Residues for which internal motion affects the measured T_1 and T_2 values were identified by an NOE of <0.65 at 5 and 15 °C, and of <0.60 at 25, 30, 33, 35, 40, and 45 °C. These included residues 3, 4, 29−32, 34, 35, 63, 66, 67, 69, and 87−89 at 5 °C, residues 3, 4, 6, 7, 11, 30−34, 51, and 66−69 at 15 °C, residues 3, 4, 6, 29−34, 51, 66, and 67 at 25 °C, residues 3, 4, 11, 29−34, 66, and 67 at 30 °C, residues 3, 4, 11, 29−31, 34, 51, 66, 67, 84, and 85 at 33 °C, residues 3, 4, 6, 11, 13, 29−35, 51, 65−67, and 85 at 35 °C, residues 3, 4, 7, 8, 13, 29−32, 34, 35, 37, 41, 51, 64−67, 69, 85, and 89 at 40 °C, and residues 3, 4, 7, 8, 10−12, 28−32, 34, 35, 37, 41, 51, 53, 59, 64, 66−68, 85, and 89 at 45 °C. The majority of these residues are located within the N-terminal helix, the turn between the N-helix and the A-helix, Ca^{2+} binding sites, the BC linker, and the C-terminus of the D-helix. Excluding these residues gives T_1/T_2 ratios of 8.4 ± 0.5, 5.2 ± 0.3, 3.5 ± 0.2, 3.0 ± 0.1, 2.8 ± 0.1, 2.6 ± 0.1, 2.3 ± 0.1, and 2.2 ± 0.1 at 5, 15, 25, 30, 33, 35, 40, and 45 °C, respectively.

Model-Independent Analysis of Backbone Dynamics. The overall correlation times at multiple temperatures were determined from the average obtained from per residue fits of the relaxation data to the Lipari−Szabo $S^2-\tau_m-\tau_f$ model (isotropic rotational tumbling), and using only relaxation data for residues with an NOE of ≥0.65 at 5 and 15 °C and an NOE of ≥0.60 at 25, 30, 33, 35, 40, and 45 °C, as previously described (*27*, *34*). The correlation times for apo-cNTnC were determined to be 3.89, 4.27, 4.79, 4.98, 5.39, 6.00, 7.85, and 10.59 ns at 45, 40, 35, 33, 30, 25, 15, and 5 °C, respectively. The correlation times follow Stokes' law; that is, the correlation times follow the experimentally determined viscosity of water over the temperature range used in this study, indicating that the protein is not subject to self-association (Figure 1).

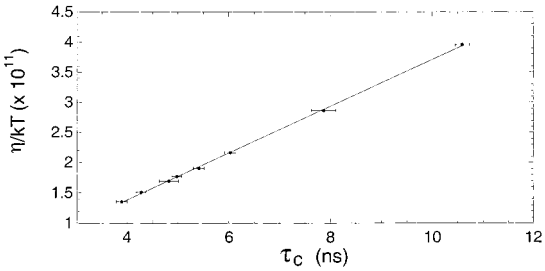

FIGURE 1: Temperature dependence of the rotational correlation time of apo-cNTnC. Stokes' law for the overall correlation time of a spherical molecule is $\tau_c = (4\pi\eta R^3)/(3kT)$, where η is the viscosity of water, R is the molecular radius, k is Boltzmann's constant, and T is temperature. The correlation time shows a linear temperature dependence on solution viscosity, as expected from Stokes' law.

A number of studies have shown that a small degree of anisotropy in the rotational tumbling of a protein can be reflected in relaxation data (*27*, *40*−*42*). For apo-cNTnC, the $D_\parallel/D_\perp$ ratio for an axially symmetric diffusion tensor was determined to be 1.12 at 30 °C (*28*), indicating that the degree of anisotropy in the rotational tumbling of apo-cNTnC is small. Values of $D_\parallel/D_\perp$ close to 1 will not affect the determination of S^2 and τ_m when assuming rotational tumbling is isotropic. The average $D_\parallel/D_\perp$ ratio determined from T_1 and T_2 data for the α-helices of apo-cNTnC at 5, 15, 25, 30, 33, 35, 40, and 45 °C is 1.02 ± 0.15 using coordinates for the average minimized structure from the ensemble of 40 solution NMR structures (*13*). The probabilities that the improvements in the fit arose by chance when assuming axially symmetric anisotropic rotational diffusion compared to isotropic rotational diffusion are 1.16×10^{-2}, 4.2×10^{-4}, 3.2×10^{-7}, 1.6×10^{-4}, 4.90×10^{-3}, 1.73×10^{-2}, 5.26×10^{-3}, and 4.08×10^{-3} at 5, 15, 25, 30, 33, 35, 40, and 45 °C, respectively. Thus, anisotropy in the rotational tumbling is only clearly apparent at 15, 25, and 30 °C, and given that the magnitude of $D_\parallel/D_\perp$ is small at these temperatures, we have used the model-independent analysis with the assumption of isotropic rotational tumbling for all temperatures. It should be noted that the structure of apo-cNTnC may be slightly different at the higher temperatures (<30 °C), and that the analysis for anisotropy in rotational tumbling was carried out using coordinates for the structure determined at 30 °C.

The average S^2 for all residues is 0.83 ± 0.15, 0.83 ± 0.10, 0.81 ± 0.09, 0.81 ± 0.08, 0.83 ± 0.10, 0.81 ± 0.08, 0.79 ± 0.08, and 0.79 ± 0.12 at 5, 15, 25, 30, 33, 35, 40, and 45 °C, respectively. Excluding N- and C-terminal residues, residue 51 in the BC linker, and residues within sites 1 and 2 gives average S^2 values of 0.88 ± 0.03, 0.86 ±

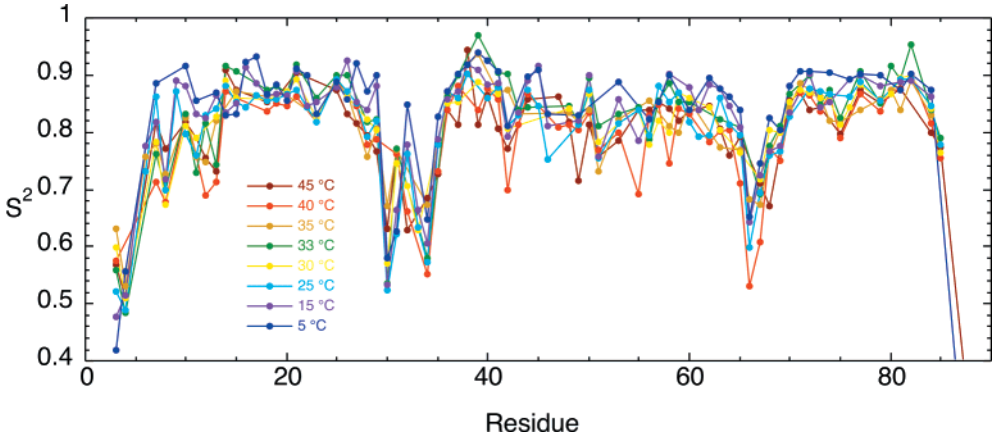

FIGURE 2: S^2 values for apo-cNTnC from 5 to 45 °C. Regions of greatest flexibility for apo-cNTnC are the N-helix (residues 5−11), a large portion of each Ca^{2+} binding site (site 1 encompasses residues 29−40, and site 2 encompasses residues 65−76), and the extreme C-terminus of the protein. Errors in S^2 have an average value of 0.01, and are not shown for clarity.

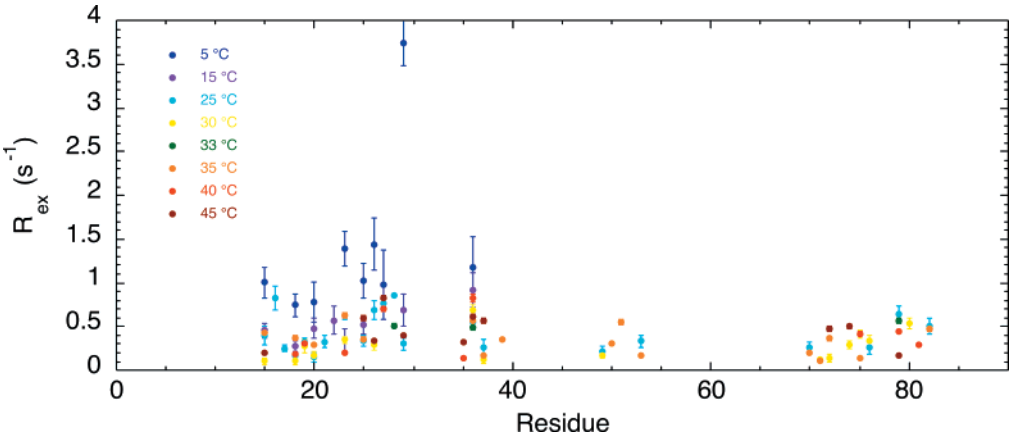

FIGURE 3: R_{ex} contributions to the transverse relaxation rate ($1/T_2$) of backbone amide ^{15}N potentially due to slow time scale (micro- to millisecond) motions from 5 to 45 °C. Several residues in the A-helix, which encompasses residues 15−27, require R_{ex} terms to fit their T_2 data properly. As discussed in the text, this is due to the unique orientation of the A-helix with respect to the unique axis of the anisotropic rotational diffusion tensor. R_{ex} terms for Leu-29 show a strong temperature dependence. Residues within the β-sheet of apo-cNTnC (35−37 and 71−73) also require R_{ex} terms to properly account for the experimental T_2 data. In addition, some residues within the D-helix require R_{ex} terms over the temperature range of 25−35 °C.

0.04, 0.84 ± 0.04, 0.84 ± 0.04, 0.86 ± 0.05, 0.84 ± 0.05, 0.82 ± 0.06, and 0.82 ± 0.05 at 5, 15, 25, 30, 33, 35, 40, and 45 °C, respectively. As shown in Figure 2, the N-terminal residues, both Ca^{2+} binding sites, and the BC interhelical region are more flexible than surrounding regions of secondary structure at all the temperatures that were employed. The C-terminal residues are also flexible. However, dynamics data for these residues are not included for temperatures above 5 °C due to overlap in the NMR spectra, except at 45 °C, where Ser-89 is resolved. It is also apparent from Figure 2 that, generally, S^2 values in regions of regular secondary structure do not display a strong temperature dependence, whereas S^2 values for flexible regions such as the termini and the Ca^{2+} binding sites exhibit greater variability with temperature.

The $S^2-\tau_m$ and $S^2-\tau_m-\tau_f$ models are not sufficient to fit the relaxation data for all residues at the various temperatures to within 95% confidence limits, taken to be 1.96 times the experimental standard deviation (*34*). In particular, several residues required either an $S^2-\tau_m-R_{ex}$ or $S^2-\tau_m-\tau_f-R_{ex}$ model (Figure 3) or a two-time scale model to account for the experimentally determined relaxation parameters to within 95% confidence limits (Figure 4). Several residues within the A-helix require the addition of an R_{ex} parameter to the expression for $1/T_2$ (Appendix, eq A2) to fit the data to within 95% confidence limits at all the temperatures that were studied. As noted previously, this is likely due to the near-parallel orientation of the A-helix with respect to the unique axis of the diffusion tensor, and not a conformational exchange phenomenon (*27*, *28*). Residue Leu-29 at the end of the A-helix exhibits a temperature-dependent R_{ex} parameter, having values of 3.7 ± 0.3, 0.8 ± 0.2, 0.3 ± 0.1, and 0.4 ± 0.1 s^{-1} at 5, 15, 25, and 45 °C, respectively. This may be due to the presence of a genuine slow (micro- to millisecond time scale) conformational exchange phenomenon. In addition, Ile-36 in the central β-sheet may be undergoing a conformational exchange phenomenon. Plots of $\ln(R_{ex})$ as a function of inverse temperature for residues 15, 18, 20, 23, and 25−27 within the A-helix and residue Leu-29 just C-terminal to the A-helix yield a mean Arrhenius activation energy of 24 kJ mol^{-1}, with a average error of 13 kJ mol^{-1}. This value is comparable to the range of activation barriers determined for reproducible R_{ex} terms for RNase H (155 residues) of ∼20−50 kJ mol^{-1} (*29*). It should be noted, however, that the linear correlation coefficient (R) or Pearson's R is 0.70, 0.64, 0.80, 0.70, 0.55, 0.90, 0.75, and 0.78 for residues 15, 18, 20, 23, 25−27, and 29, respectively, indicating that the calculated lines (excluding residue 26) generally do not fit

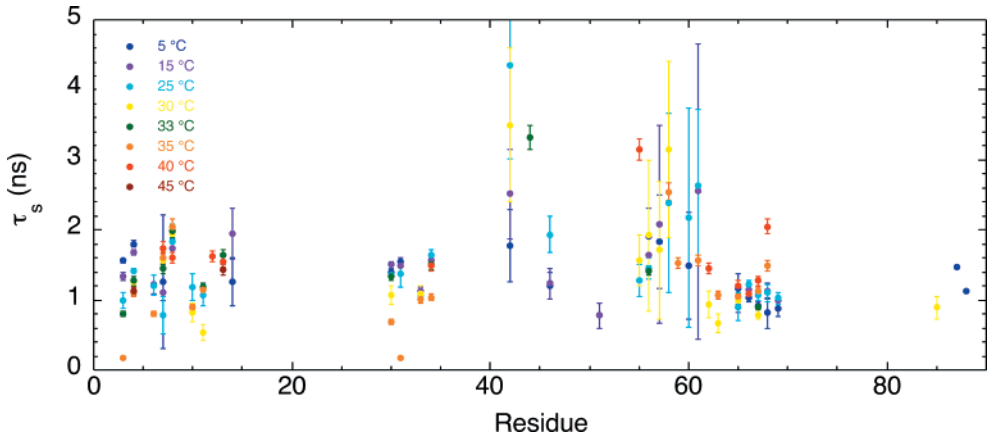

FIGURE 4: Correlation times for slow nanosecond time scale internal motions (τ_s) for apo-cNTnC from 5 to 45 °C. Residues within the N-helix and site 1, residues 42 and 46, residue Asn-51 in the BC-linker, several residues in the C-helix, site 2, and the C-terminus require the two-time scale internal motion model to properly account for their relaxation data. The τ_s values for the C-helix have large errors in comparison to errors in τ_s for other regions of apo-cNTnC.

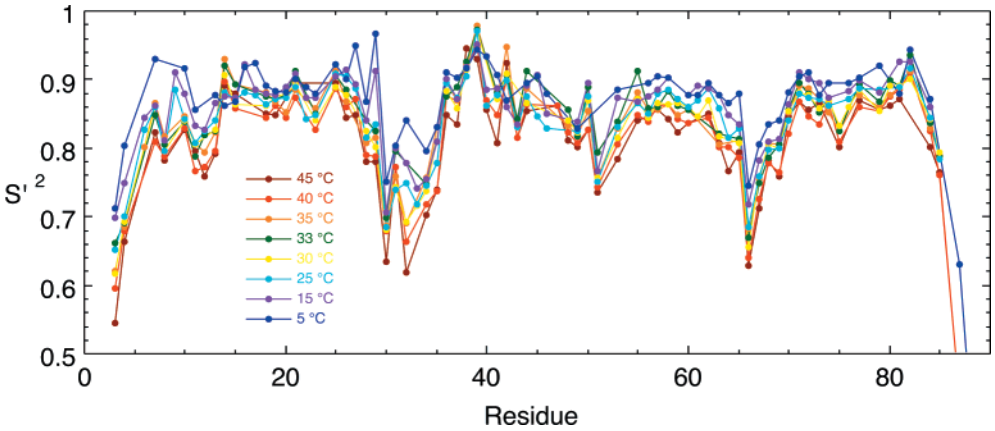

FIGURE 5: S'^2 values for apo-cNTnC from 5 to 45 °C. The pattern of values S'^2 is similar to that for S^2 values obtained using the Lipari−Szabo model-independent analysis. Regions of enhanced flexibility, with respect to regions of regular secondary structure for apo-cNTnC, are the N-helix (residues 5−11), a large portion of each Ca^{2+} binding site (site 1 encompasses residues 29−40, and site 2 encompasses residues 65−76), and the extreme C-terminus of the protein. Note that residues requiring R_{ex} terms when using the Lipari−Szabo model-independent analysis show elevated values of S'^2 with respect to the Lipari−Szabo S^2 values. Errors in S'^2 have an average value of 0.01, and are not shown for clarity.

the original data very well, as the R value ranges from 0 to 1 with values near 1 indicating a better fit. In addition, many of the R_{ex} terms for residues in the A-helix are less than 0.5 s^{-1}, and values of this magnitude this should be interpreted with caution (*29*). Thus, it is likely that R_{ex} terms for residues within the A-helix are a result of rotational diffusion anisotropy, despite the fact that anisotropy in the rotational tumbling is only readily apparent at 15, 25, and 30 °C.

Several residues required model 5 (*43*) to account for relaxation parameters at the various temperatures to within 95% confidence limits (Figure 4). These include residues at the N- and C-termini, in Ca^{2+} binding sites 1 and 2, and in the C-helix. In addition, residues within the N-helix required a two-time scale model as well. For residues in the N-helix, polypeptide termini, and Ca^{2+} binding sites, the requirement for a two-time scale model likely reflects motion on multiple time scales in these regions. However, for the C-helix, the two-time scale model is necessary to fit the data appropriately due to the nearly 90° orientation of this helix with respect to the unique axis of the diffusion tensor. Interestingly, this was difficult to pinpoint in previous studies (*28*), as only one or two residues required the two-time scale model, and the requirement was not consistent between data sets collected at 500 and 600 MHz. However, as shown in Figure 4, when the large errors associated with τ_s are considered, the requirement for a two-time scale model to account for relaxation data of the C-helix is likely an artifact arising from anisotropic rotational diffusion.

Temperature Dependence of S^2 Values and Calculation of Heat Capacity Contributions from Backbone Amide N−NH Vector Motions. Contributions to the heat capacity from picosecond to nanosecond time scale backbone $^{15}N-^{1}H_N$ vector fluctuations in apo-cNTnC were estimated from eqs 1 and 2 using S'^2 values (Figure 5) and presented in Figure 7. In addition, we determined values of $d(1 - \sqrt{S^2})/dT$ (using S'^2 values) for comparison to $C_{p,j}$ values (Figure 6). Generally, the slopes $d(1 - \sqrt{S'^2})/dT$ and $\partial[S_{p,j}(T)]/\partial[\ln(T)]$ are quite small and difficult to determine precisely, as S^2 values for the folded state of a protein are generally not strongly temperature dependent (Figures 6 and 7). Thus, we selected values of $d(1 - \sqrt{S'^2})/dT$ and $C_{p,j}$ by trimming the data as follows. Residues for which relaxation data were available for less than four temperatures were excluded from the analysis; in addition, residues for which the error in the linear least-squares fit was greater than one standard deviation from the mean for all residues were also excluded. The averaged trimmed values of $d(1 - \sqrt{S'^2})/dT$ and $C_{p,j}$ are 8 $\times 10^{-4}$ K^{-1} and 6 cal mol^{-1} K^{-1} per residue, respectively,

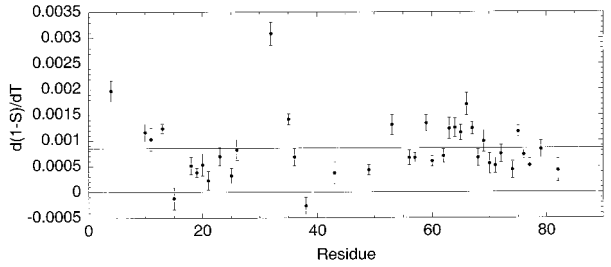

FIGURE 6: Values of $d(1 - \sqrt{S'^2})/dT$ plotted with respect to the sequence of apo-cNTnC. The average value of $\sim 8 \times 10^{-4}$ K^{-1} for $d(1 - \sqrt{S'^2})/dT$ is indicated on the plot. As S'^2 values are not strongly temperature dependent for a folded protein, $d(1 - \sqrt{S'^2})/dT$ is small, and difficult to measure; thus, only the most reliable values of $d(1 - \sqrt{S'^2})/dT$ are presented (see the text).

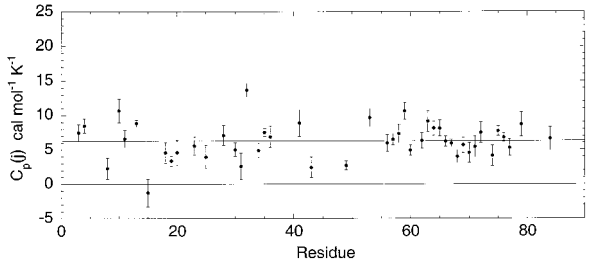

FIGURE 7: Heat capacities ($C_{p,j}$) calculated from backbone amide S'^2 values. The average $C_{p,j}$ is $\sim$6 cal mol^{-1} K^{-1} and is indicated on the plot. As is the case for $d(1 - \sqrt{S'^2})/dT$ values, only the most reliable values of $C_{p,j}$ are shown on the plot.

with average errors of 2×10^{-4} K^{-1} and 3 cal mol^{-1} K^{-1}, respectively. The averaged trimmed value of $d(1 - \sqrt{S'^2})/dT$ determined in this study compares quite favorably with the average value of $(5.9 \pm 0.7) \times 10^{-4}$ K^{-1} determined for RNase H (*29*), for residues in regions of secondary structure, excluding residues undergoing chemical exchange. For the E140Q mutant of the C-terminal domain of calmodulin (E140Q TR2C), another EF hand family Ca^{2+} binding protein, the weighted mean value of $C_{p,j}$ was found to be 2 ± 5 cal mol^{-1} K^{-1} per residue (*44*), and this value compares favorably to the trimmed $C_{p,j}$ determined in this study. For the B1 domain from *Streptococcal* protein G, the average 10% trimmed value of $C_{p,j}$ for all residues is 11 ± 3 cal mol^{-1} K^{-1} per residue (*45*), and somewhat larger than that found in this study.

Thermal Denaturation Monitored by Circular Dichroism. Figure 8 shows the temperature-induced thermal denaturation curve for apo-cNTnC. At 5 °C, the mean residue ellipticity of -33980 deg cm^2 dmol^{-1} is expected for apo-cNTnC, a highly α-helical protein (*13*). The denaturation curve shows a cooperative unfolding of apo-cNTnC, with a melting temperature ($T°$) of 68.8 °C. Figure 8 indicates that the population of the unfolded state is less than 5% over the temperature range used in this study.

DISCUSSION

Slow Time Scale Internal Motions: N-Terminal Residues and the N-Helix. For the ensemble of solution NMR structures for apo-cNTnC, residues 5−11 form a regular α-helix and residues Asp-3 and Ile-4 are unstructured (*13*). However, the dynamics of the N-terminal residues and N-terminal helix as determined from the ^{15}N NMR relaxation data presented here show panoplies of motions and richness in detail. Relaxation data for Asp-3 require a two-time scale

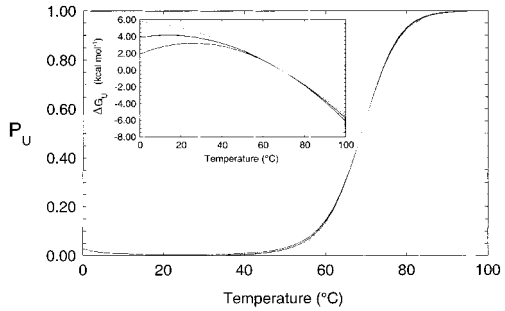

FIGURE 8: Temperature-induced thermal denaturation of apo-cNTnC. Ellipticity readings were monitored at 222 nm (in millidegrees) in 50 mM potassium phosphate, 100 mM KCl, 15 mM DTT, and 15 mM EDTA (pH 6.7). The fitted parameters are as follows: $T°$ (melting temperature) = 342 K, $\Delta H_U°$ (apparent enthalpy of unfolding at $T°$) = 50.2 kcal mol^{-1}, and $\Delta C_{p,U}$ (temperature-independent heat capacity of unfolding) = 0.84 kcal mol^{-1} K^{-1}. The inset graph shows the corresponding stability curves obtained from nonlinear least-squares fitting of the data shown in the main graph. The inset graph shows $\Delta G_U(T)$ (the temperature dependence of the free energy of unfolding) curves calculated for $\Delta C_{p,U}$ (middle curve), $\Delta C_{p,U}$ plus one standard deviation of the fit (bottom curve), and $\Delta C_{p,U}$ minus one standard deviation of the fit (top curve). The temperature dependence of the population of the unfolded state [$P_U(T)$] shows that apo-cNTnC is stable over the temperature range employed in this study (5−45 °C).

model at 5, 15, 25, and 33 °C. At 30, 35, 40, and 45 °C, the $S^2-\tau_m-\tau_f$ model is sufficient to fit the relaxation data to within 95% confidence limits. The order parameter for model 5 includes slow internal motions that occur on two time scales ($S^2 = S_s^2 S_f^2$, where S_s^2 is the order parameter for slow internal motions and S_f^2 is the order parameter for fast internal motions) and shows an increase with increasing temperature for Asp-3. For example, S^2 is 0.418 ± 0.009, 0.477 ± 0.017, 0.521 ± 0.021, and 0.559 ± 0.033 at 5, 15, 25, and 33 °C, respectively. Nanosecond time scale internal motions do not contribute to the relaxation properties of the backbone amide ^{15}N of Asp-3 at 30, 35, 40, and 45 °C, and the $S^2-\tau_m-\tau_f$ model is sufficient to account for the relaxation data for Asp-3 to within 95% confidence limits. The correlation time for slow internal motions (τ_s) decreases from 1.56 ± 0.03 ns at 5 °C to 1.33 ± 0.06, 1.00 ± 0.11, and 0.80 ± 0.20 ns at 15, 25, and 33 °C, respectively. The results for τ_s indicate that with increasing temperature, slow nanosecond time scale internal motions become progressively negligible, and the limit is approached where $\tau_s = 0$ at 35, 40, and 45 °C for Asp-3. However, the results for S^2 at 5, 15, 25, and 33 °C indicate that the backbone amide ^{15}N−^{1}H$_N$ vector for this residue becomes less flexible with increasing temperature. It is difficult to rationalize a decrease in flexibility with increasing temperature, and we have found that the two-time scale model is unreliable for extracting meaningful values of S^2 as a function of temperature, at a single magnetic field strength, and as presently implemented with the assumption $\tau_f \rightarrow 0$. Instead, we have utilized the approach of Schurr et al. (*25*, *39*) for extracting values of S'^2 that can be used in a quantitative manner. Using this approach, we find $S'^2 = 0.712 \pm 0.007$, 0.70 ± 0.01, 0.65 ± 0.01, and 0.66 ± 0.01 at 5, 15, 25, and 33 °C, respectively, for Asp-3. Thus, S'^2 shows the expected decrease with increasing temperature. The values of S^2 obtained from the $S^2-\tau_m-\tau_f$ model (using a single global value for τ_m) are 0.598 ± 0.007, 0.63 ± 0.01, 0.58 ± 0.01, and 0.57 ± 0.02 at 30, 35, 40, and 45 °C, respectively, and agree with the

value of 0.62 ± 0.01 obtained at 30 and 35 °C, and 0.60 ± 0.02 and 0.54 ± 0.02 at 40 and 45 °C, respectively, using the approach of Schurr et al. (*39*). Relaxation data were fit to the $S'^2-\tau'_m-\tau'_f$ model, and errors for these parameters were estimated from Monte Carlo analysis using the program Mathematica (*46*).

For Ile-4, the two-time scale model is required to fit relaxation data acquired at 5−35 °C. S^2 is 0.557 ± 0.007 at 5 °C and 0.515 ± 0.011, 0.489 ± 0.005, 0.510 ± 0.008, 0.485 ± 0.015, 0.531 ± 0.013, and 0.510 ± 0.044 at 15, 25, 30, 33, 35, and 45 °C, respectively. The correlation time for slow internal motions (τ_s) decreases from 1.80 ± 0.05 ns at 5 °C to 1.66 ± 0.04, 1.42 ± 0.03, 1.26 ± 0.04, 1.27 ± 0.07, 1.09 ± 0.07, and 1.1 ± 0.2 ns at 15, 25, 30, 33, 35, and 45 °C, respectively. Arrhenius plots of $\ln(\tau_s)$ as a function of inverse temperature yield activation energies for slow internal motions of ∼17 and ∼10 kJ mol^{-1} for Asp-3 and Ile-4, respectively, with linear correlation coefficients (R) of 0.99 and 0.96, respectively. However, these activation energies are rough estimates because the details of the underlying motions are unknown, and that the two-time scale model (as presently implemented with $\tau_f \rightarrow 0$, Appendix, eq A5) is somewhat unreliable since it contains zero degrees of statistical freedom (*29*).

The results for Asp-3 and Ile-4 are likely to be a general feature for N-terminal residues in proteins that are not constrained by disulfide bridges or found at domain or protein−protein or protein−ligand interfaces, for example. Apart from Asp-3 and Ile-4, residues 6−8, 10, and 11 require the two-time scale model that includes nanosecond internal motions to fit the relaxation data to within 95% confidence limits at various temperatures. The correlation times for these motions range from 0.7 to 1.8 ns at 35 °C without a clear dependence on temperature. At 5 °C, relaxation data for residues 10 and 11 are properly accounted for by the $S^2-\tau_m-\tau_f$ model, whereas at 25, 30, and 35 °C for residue 10 and at 25, 30, 33, and 35 °C for residue 11, the two-time scale model is required to account for the relaxation data. At 40 and 45 °C, residues 10 and 11 require the $S^2-\tau_m-\tau_f$ model. These results indicate that slow nanosecond time scale motions are "frozen" at 5 and 15 °C for the C-terminal end of the N-helix; with increasing temperature, slow time scale motions become evident, and the rates of these motions increase with temperature to the extent that a switch from model 5 to model 2 is seen when the temperature is increased from 40 to 45 °C.

Slow Time Scale Internal Motions: Ca^{2+} Binding Site 1. Positions 2−6 of the 12-residue EF hand Ca^{2+} binding site1 of apo-cNTnC are the most flexible in the site, as determined by ^{15}N NMR relaxation, as determined in this and previous studies (*28*). A 5, 15, and 25 °C, residues Gly-30, Ala-31, Asp-33, and Gly-34 (positions 2, 3, 5, and 6, respectively) require the two-time scale model for internal motions to account for their relaxation data. The τ_s values for these residues range, on average, from 1.4 ns for Gly-30, to 1.5 ns for Ala-31, to 1.1 ns for Asp-33, to 1.6 ns for Gly-34 at 5, 15, and 25 °C. Interestingly, τ_s does not show a clear dependence on temperature at 5, 15, and 25 °C for these residues. At 30 °C, Gly-30 relaxation data are fit with the two-time scale model where $\tau_s = 1.1$ ns, and at 35 and 45 °C, the relaxation data for Gly-30 are properly accounted for by the $S^2-\tau_m-\tau_f$ model. For Ala-31, the $S^2-\tau_m-\tau_f$ model is sufficient to account for the relaxation data from 30 to 45 °C. Relaxation data for Asp-33 were not available at 5 and 33−45 °C due to overlap in the NMR spectra, and at 15, 25, and 30 °C, the two-time scale model for internal motion is required to fit the data with τ_s values of 1.1 ns at these temperatures. Relaxation data for Gly-34 are not fit by any spectral density model at 30 °C. At 33, 35, and 40 °C, the two-time scale model is required to fit the relaxation data with τ_s ranging from 1 to 1.5 ns, and at 45 °C, the $S^2-\tau_m-\tau_f$ model is sufficient to account for the relaxation data. Interestingly, relaxation data for Glu-32 are fit to within 95% confidence limits with the $S^2-\tau_m-\tau_f$ model for all temperatures apart from 35 °C, for which data are not available due to spectral overlap. Thus, the most flexible residues in site 1 (positions 2−6) are undergoing nanosecond time scale motions, and increasing temperature causes these motions to contribute less to the NMR relaxation of the backbone amide ^{15}N (approach the limit $\tau_s = 0$).

Slow Time Scale Internal Motions: Ca^{2+} Binding Site 2. As for site 1, positions 2−6 of site 2 are the most flexible in the functional Ca^{2+} binding site. As in site 1, most residues in positions 2−6 require the two-time scale model to properly account for the relaxation data at the lower temperatures (5, 15, and 25 °C). However, positions 2, 3, and 6 in site 2 are less flexible than in site 1. For example, τ_s values are on average about 1.0 and 1.1 ns with corresponding average S^2 values of 0.63 and 0.72 for positions 2 and 3 (Glu-66 and Asp-67, respectively) in site 2 compared to τ_s values of 1.4 and 1.5 ns and S^2 values of 0.56 and 0.64 for site 1 at 5, 15, and 25 °C. For position 6 in site 2 (Gly-70), the two-time scale model is required only at 15 °C. However, at this temperature, $\tau_s = 2.9 \pm 2.4$ ns, indicating that this model is not meaningful at this temperature. In comparison, the average τ_s for position 6 in site 1 (Gly-34) at 5, 15, and 25 °C is 1.6 ns. Additionally, the average S^2 value at 5, 15, and 25 °C for position 6 in site 2 is 0.85 compared to 0.61 for site 1. Interestingly, a different picture emerges for a comparison of site 1 and site 2 dynamics using S'^2 values. For positions 2 and 3 (Gly-30 and Ala-31 in site 1 and Glu-66 and Asp-67 in site 2, respectively), S'^2 values are very similar, whereas position 6 has lower values of S'^2 for site1 than for site 2.

Values of $d(1 - \sqrt{S'^2})/dT$ and $C_{p,j}$ from Backbone Amide $^{15}N-^1H_N$ Vector Motions: Comparison to Results from Other Proteins. The average value of $d(1 - \sqrt{S'^2})/dT$ for flexible residues in the trimmed data set from the N-terminus, the turn between helices N and A, the linker between helices B and C, and Ca^{2+} binding sites 1 and 2 (residues 4, 13, 32, 49, 53, and 66−69) is (14.0 ± 0.6) × 10^{-4} K^{-1}. The average value of $d(1 - \sqrt{S'^2})/dT$ for residues in regions of secondary structure, the N-, A-, B-, C-, and D-helices, and the β-sheet is (6.9 ± 0.3) × 10^{-4} K^{-1}. These results are consistent with previous studies indicating that the response of S^2 to temperature is greater for flexible residues than for regions involved in regular secondary structure within a protein (*25, 29, 44*). For example, for RNase H, the average $d(1 - \sqrt{S^2})/dT$ for residues in regions of secondary structure (excluding residues undergoing significant chemical exchange) is (5.9 ± 0.7) × 10^{-4} K^{-1}, and for the loop and C-terminal regions, $d(1 - \sqrt{S^2})/dT$ ranges from ∼2 × 10^{-3} to 4 × 10^{-3} K^{-1} (*29*).

The average heat capacity for residues in regions of secondary structure, the N-, A-, B-, C-, and D-helices, and the β-sheet in apo-cNTnC using trimmed data is 6.2 ± 0.3 cal mol^{-1} K^{-1}. The average heat capacity for flexible residues in apo-cNTnC is 6.4 ± 0.3 cal mol^{-1} K^{-1} (residues 3, 4, 13, 30−32, 34, 49, 53, and 66−70). Although it appears as though structured and flexible residues have about the same heat capacity, the average heat capacity of 8 cal mol^{-1} K^{-1} (with an average standard deviation of 1.1 cal mol^{-1} K^{-1}) determined for the N-terminal residues (Asp-3 and Ile-4) of apo-cNTnC compares favorably with the value of $\sim 9 \pm \sim 2$ cal mol^{-1} K^{-1} measured for the N-terminal residues of E140Q TR2C (*44*). Note that the error for the weighted average of the heat capacity for the N-terminal residues of E140Q TR2C is the standard error, or standard deviation of the mean; the standard deviation of a single $C_{p,j}$ value is likely to be higher. Additionally, the average heat capacity for the A-helix in apo-cNTnC is 4 cal mol^{-1} K^{-1} (with an average standard deviation of 1.5 cal mol^{-1} K^{-1}), and this value also compares with that measured for the analogous E-helix in E140Q TR2C of approximately -1 ± 1 cal mol^{-1} K^{-1} (error bars indicate the standard error). Thus, in comparison to similar studies involving RNase H (*29*) and E140Q TR2C (*44*), we have reached the same conclusions in this study, namely, that flexible residues have higher heat capacities than residues involved in regular secondary structure such as α-helix and β-sheet. Physically, this means that flexible residues can access a larger number of conformational states thermally than more rigid residues such as those involved in secondary structure.

The results in this paper differ from those of a study of the temperature dependence of backbone amide ^{15}N−^{1}H$_N$ dynamics of the B1 domain from *Streptococcal* protein G, a small 56-residue protein (*45*). In that study, it was concluded that the motions of the ^{15}N−^{1}H$_N$ groups in regions of regular secondary structure of the B1 domain are substantially more dependent on temperature than the temperature dependence observed for RNase H and E140Q TR2C. The temperature dependence of backbone amide ^{15}N−^{1}H$_N$ dynamics and correlation with regions of secondary structure observed for apo-cNTnC in this paper are consistent with those reported for RNase H (*29*) and E140Q TR2C (*44*). For the B1 domain, it is believed that the higher per residue backbone heat capacity determined from ^{15}N relaxation contributes to the higher thermal stability of this protein compared to RNase H, and E140Q TR2C, and the results for apo-cNTnC presented herein. The thermal denaturation temperatures ($T°$) of RNase H and apo-cNTnC are 66 and 68 °C, respectively, whereas $T°$ is 87 °C for the B1 domain. The change in heat capacity for the unfolding transition $\Delta C_{p,U}$ is 2.9, 3.5, and 11.3 kJ mol^{-1} K^{-1} for the B1 domain, apo-cNTnC, and RNase H, respectively. As pointed out by Seewald et al. (*45*), these $\Delta C_{p,U}$ values reflect differences in buried, nonpolar surface area between the respective proteins. Compared to that of the B1 domain, increases in buried nonpolar surface area are 1.2- and 2.9-fold for apo-cNTnC and RNase H, respectively. The buried nonpolar surface area is $\sim$2900, 3375, and 8700 Å^2 for the B1 domain, apo-cNTnC, and RNase H, respectively. However, it is estimated that if the per residue backbone heat capacity of the B1 domain is similar to that measured for RNase H, E140Q TR2C, and apo-cNTnC (this study), then $T°$ would be lowered by 9 °C, as $\Delta C_{p,U}$ would be increased (thermal destabilization). Thus, it is suggested that the ordered secondary structure regions within the B1 domain contribute more to the conformational heat capacity than those in RNase H and E140Q TR2C and, given the results in this study, apo-cNTnC as well. Interestingly, backbone amide ^{15}N−^{1}H$_N$ S^2 values for the B1 domain are lower than expected ($S^2 \sim 0.85$) at 30 °C for regions of well-defined secondary structure in proteins. This result is consistent with the hypothesis that the B1 domain relies on backbone flexibility to maintain thermal stability. Further work from the Stone group, involving measurement of backbone amide ^{15}N dynamics of three different single-residue mutants of the B1 domain, each possessing a wide range of stability, lends further support to the suggestion that backbone conformational entropy can contribute to the thermal stability of this small protein (*47*). In particular, the most stable mutant appears to have the highest backbone flexibility.

Determination of the contribution of changes in entropy for the side chains from the B1 domain to the heat capacity may, in the future, significantly improve the understanding of the role of dynamics in the determination of stability for this protein. One might expect that modulation of side chain entropy, especially pico- to nanosecond time scale motion, is a more plausible mechanism for fine-tuning the stability of a protein, rather than modulation of pico- to nanosecond time scale protein backbone dynamics, particularly increased backbone flexibility for increased thermal stability. Indeed, with respect to protein−protein interactions, the Wand group has shown that a decrease in the amplitude of pico- to nanosecond time scale side chain dynamics of Ca^{2+}-saturated calmodulin is an important factor for achieving functionally relevant enthalpy−entropy compensation in the formation of the Ca^{2+}-saturated calmodulin−smooth muscle myosin light chain kinase (smMLCK) peptide complex, whereas the pico- to nansecond time scale motions of the backbone were found to be unchanged with respect to peptide binding (*48*). Additionally, several studies have indicated that micro- to millisecond time scale motions of the protein backbone within or in the vicinity of the binding interface may be particularly important in determination of the affinity of protein−ligand interactions, and often, these motions are quenched upon ligand binding (*49*−*52*). What is clear in many of the aforementioned studies is that flexibility in the ligand-free state is likely to be important for determining affinity constants and binding specificity. Often, backbone flexibility is diminished upon ligand binding, and the entropic cost is offset by formation of favorable enthalpic interactions. In contrast, increased backbone conformational entropy upon hydrophobic ligand binding, determined through changes in pico- to nanosecond time scale fluctuations, has been observed for binding of the small, hydrophobic pheromonal ligand 2-*sec*-butyl-4,5-dihydrothiazole to mouse major urinary protein-I (*53*). It is suggested that due to the fact that the ligand is small and hydrophobic, enthalpic contributions to the free energy may not be sufficient to overcome any unfavorable effects of binding; thus, subtle changes in protein structure allow for an increase in the backbone conformational entropy of the protein, contributing to favorable binding.

The majority of studies involving determination of heat capacity from backbone amide ^{15}N NMR relaxation to date,

including the results of this study, indicate that for regions of well-defined secondary structure, the response of pico- to nanosecond time scale fluctuations of the backbone to temperature is small (~6 cal mol^{-1} K^{-1} per residue), and for flexible regions, the heat capacity increases to ~9 cal mol^{-1} K^{-1} per residue. These results are consistent with a view in which flexible regions of the polypeptide backbone can access a larger number of states thermally, whereas more structured regions can access fewer states thermally. At present, one study stands out, where the backbone of the B1 domain from *Streptococcal* protein G was shown to rely on increased heat capacity for residues involved in well-defined secondary structure, and that this was critical for maintaining the high thermal stability of this protein.

Relevance of Backbone Heat Capacity with Respect to Function. In previous studies, it has been demonstrated that the conformational entropy difference between sites 1 and 2 of apo-sNTnC is similar to the free energy difference of Ca^{2+} binding between the sites, and this is consistent with the idea that site 2 binds Ca^{2+} prior to site 1 due to its greater rigidity (*27*, *28*). In this study, we have determined that the average heat capacities for the most flexible residues (positions 2−6) in Ca^{2+} binding sites 1 and 2 of cNTnC are statistically different, having values of 6.6 ± 0.7 and 5.3 ± 0.4 cal mol^{-1} K^{-1}, respectively. These results indicate that site 2 accesses fewer conformational states thermally than site 1. The implication is that the larger heat capacity for site 1 relative to that for site 2 is a potential mechanism for EF hand proteins that can contribute directly to Ca^{2+} affinity differences between sites. Given that TnC proteins experience conformational changes upon Ca^{2+} binding, the heat capacity difference between Ca^{2+} binding sites can also contribute directly to the function of these proteins. While site 1 naturally does not bind Ca^{2+} in the cardiac isoform of TnC, it is interesting that the sites remain thermodynamically coupled, and we feel that the difference in heat capacity between sites for apo-cNTnC is a mechanism that will likely modulate differences in Ca^{2+} affinity in EF hand proteins with two active Ca^{2+} binding sites.

ACKNOWLEDGMENT

We thank David Corson and Linda Saltibus for assistance in preparation of cNTnC samples, Professor Lewis E. Kay for providing pulse sequences and relaxation data analysis software, Gerry McQuaid for maintenance of NMR spectrometers, and Leigh Willard and Robert Boyko for computer expertise.

APPENDIX

Relaxation parameters for a backbone amide $^{15}N-^{1}H_N$ pair (^{15}N-T_1, ^{15}N-T_2, and $\{^{1}H\}-^{15}N$ NOE) are determined predominantly by magnetic dipole interactions between the amide ^{15}N nucleus and the ^{1}H, and by anisotropy for the chemical shift of the ^{15}N nucleus. Expressions for ^{15}N-T_1, ^{15}N-T_2, and $\{^{1}H\}-^{15}N$ steady-state NOE relaxation parameters are well-established and are given by linear combinations of the spectral density function [$J(\omega)$] at the Larmor angular frequencies, and linear combinations thereof, for ^{15}N and $^{1}H_N$ nuclei (*54*):

$$\frac{1}{T_1} = D[J(\omega_H - \omega_N) + 3J(\omega_N) + 6J(\omega_H + \omega_N)] + C[J(\omega_N)] \quad \text{(A1)}$$

$$\frac{1}{T_2} = \frac{D}{2}[4J(0) + J(\omega_H - \omega_N) + 3J(\omega_N) + 6J(\omega_H + \omega_N) + 6J(\omega_H)] + C\left[\frac{2}{3}J(0) + \frac{1}{2}J(\omega_N)\right] \quad \text{(A2)}$$

$$\text{NOE} = 1 + \frac{\gamma_H}{\gamma_N}\left\{\frac{D[6J(\omega_H + \omega_N) - J(\omega_H - \omega_N)]}{1/T_1}\right\} \quad \text{(A3)}$$

where $D = (\mu_0/4\pi)^2[(\gamma_H^2\gamma_N^2\hbar^2)/(4r_{NH}^6)]$ and $C = [(\Delta^2\omega_N^2)/3]$, μ_0 is the permeability constant of free space ($4\pi \times 10^{-7}$ kg m s^{-2} A^{-2}), γ_H is the proton magnetogyric ratio (2.68×10^8 rad s^{-1} T^{-1}), γ_N is the magnetogyric ratio of ^{15}N (-2.71×10^7 rad s^{-1} T^{-1}), r_{NH} is the proton−nitrogen internuclear separation (102 pm), Δ is the difference between the parallel and perpendicular components of the ^{15}N chemical shift tensor (−160 ppm), and $\hbar$ is Planck's constant divided by 2π (1.05×10^{-34} J s). In the Lipari−Szabo analysis, the spectral density is formulated in terms of an order parameter (S^2) that indicates the degree of spatial restriction for a backbone amide $^{15}N-^{1}H_N$ bond vector, with an associated internal correlation time, and with the assumption of a single, global molecular rotational correlation time:

$$J(\omega) = \frac{2}{5}\left[\frac{S^2\tau_m}{1 + \omega^2\tau_m^2} + \frac{(1 - S^2)\tau}{1 + \omega^2\tau^2}\right] \quad \text{(A4)}$$

where $\tau^{-1} = \tau_m^{-1} + \tau_f^{-1}$, S^2 is the generalized order parameter, τ_m is the correlation time for overall molecular tumbling, and τ_f is the correlation time for internal motion. Additionally, a heuristic model, which has not been derived rigorously and which accounts for internal motions that occur on two time scales, can be employed to analyze relaxation data. This model is comprised of an order parameter for fast picosecond internal motions (S_f^2), an order parameter for nanosecond time scale internal motions faster than τ_m but slower than τ_f (S_s^2), a correlation time for picosecond internal motions (τ_f), and a correlation time for nanosecond internal motions (τ_s):

$$J(\omega) = \frac{2}{5}\left[\frac{S^2\tau_m}{1 + \omega^2\tau_m^2} + \frac{(S_f^s - S^2)\tau_s'}{1 + \omega^2\tau_s'^2}\right] \quad \text{(A5)}$$

where $S^2 = S_f^2S_s^2$ and $\tau_s' = \tau_s\tau_m/(\tau_s + \tau_m)$. Note that for eq A5, it is assumed that fast time scale motions do not contribute to relaxation ($\tau_f \rightarrow 0$). For each residue, parameters for each model of the spectral density function were adjusted to minimize the objective function given in eq A6, using software provided by L. E. Kay.

$$\chi^2 = \frac{(T_{1,c} - T_{1,e})^2}{\sigma_{T_1}^2} + \frac{(T_{2,c} - T_{2,e})^2}{\sigma_{T_2}^2} + \frac{(\text{NOE}_c - \text{NOE}_e)^2}{\sigma_{\text{NOE}}^2} \quad \text{(A6)}$$

where the subscripts c and e indicate calculated and experimental values, respectively, and σ is the error of the individual relaxation parameters.

For the analysis of rotational diffusion anisotropy with an axially symmetric diffusion tensor, the following form of the spectral density function was employed (*55*−*57*):

$$J(\omega) = \frac{2}{5} S_f^2 \sum_{3}^{j=1} A_j \left[\frac{S_s^2 \tau_j}{1 + \omega^2 \tau_j^2} + \frac{(1 - S_s^2)\tau_j'}{1 + \omega^2 \tau_j'^2} \right] \quad \text{(A7)}$$

where $\tau_j' = \tau_s \tau_j / (\tau_s + \tau_j)$, $\tau_1^{-1} = 6D_\perp$, $\tau_2^{-1} = 5D_\perp + D_\parallel$, $\tau_3^{-1} = 2D_\perp + 4D_\parallel$, $A_1 = (3 \cos^2 \theta - 1)^2/4$, $A_2 = 3 \cos^2 \theta \sin^2 \theta$, $A_3 = {}^3/_4 \sin^4 \theta$, and θ is the angle between the $^{15}N-^1H_N$ bond vector and the unique axis of the diffusion tensor in the principal axis system.

REFERENCES

1. Tobacman, L. S. (1996) *Annu. Rev. Physiol. 58*, 447−481.
2. Squire, J. M., and Morris, E. P. (1998) *FASEB J. 12*, 761−771.
3. Gordon, A. M., Homsher, E., and Regnier, M. (2000) *Physiol. Rev. 80*, 853−924.
4. Herzberg, O., and James, M. N. G. (1988) *J. Mol. Biol. 203*, 761−779.
5. Satyshur, K. A., Rao, S. T., Pyzalska, D., Drendal, W., Greaser, M., and Sundralingham, M. (1988) *J. Biol. Chem. 263*, 1628−1647.
6. Slupsky, C. M., and Sykes, B. D. (1995) *Biochemistry 34*, 15953−15964.
7. van Eerd, J.-P., and Takahashi, K. (1975) *Biochem. Biophys. Res. Commun. 64*, 122−127.
8. Putkey, J. A., Sweeny, H. L., and Campbell, S. T. (1989) *J. Biol. Chem. 264*, 12370−12378.
9. Gagné, S. M., Tsuda, S., Li, M. X., Smillie, L. B., and Sykes, B. D. (1995) *Nat. Struct. Biol. 2*, 784−789.
10. Strynadka, N. C., Cherney, M., Sielecki, A. R., Li, M. X., Smillie, L. B., and James, M. N. (1997) *J. Mol. Biol. 273*, 238−255.
11. Houdusse, A., Love, M. L., Dominguez, R., Grabarek, Z., and Cohen, C. (1997) *Structure 5*, 1695−1711.
12. Sia, S. K., Li, M. X., Spyracopoulos, L., Gagné, S. M., Liu, W., Putkey, J. A., and Sykes, B. D. (1997) *J. Biol. Chem. 272*, 18216−18221.
13. Spyracopoulos, L., Li, M. X., Sia, S. K., Gagné, S. M., Chandra, M., Solaro, R. J., and Sykes, B. D. (1997) *Biochemistry 36*, 12138−12146.
14. Li, M. X., Spyracopoulos, L., and Sykes, B. D. (1999) *Biochemistry 38*, 8289−8298.
15. McKay, R. T., Saltibus, L. F., Li, M. X., and Sykes, B. D. (2000) *Biochemistry 39*, 12731−12738.
16. Wagner, G. (1993) *Curr. Opin. Struct. Biol. 3*, 748−753.
17. Palmer, A. G. (1993) *Curr. Opin. Biotechnol. 4*, 385−391.
18. Kay, L. E. (1998) *Nat. Struct. Biol. 5*, 513−517.
19. Lipari, G., and Szabo, A. (1982) *J. Am. Chem. Soc. 104*, 4546−4559.
20. Lipari, G., and Szabo, A. (1982) *J. Am. Chem. Soc. 104*, 4559−4570.
21. Kay, L. E., Torchia, D. A., and Bax, A. (1989) *Biochemistry 28*, 8972−8979.
22. Akke, M., Bruschweiler, R., and Palmer, A. G. (1993) *J. Am. Chem. Soc. 115*, 9832−9833.
23. Li, Z., Raychaudhuri, S., and Wand, A. J. (1996) *Protein Sci. 5*, 2647−2650.
24. Yang, D., and Kay, L. E. (1996) *J. Mol. Biol. 263*, 369−382.
25. Yang, D., Mok, Y.-K., Forman-Kay, J. D., Farrow, N. A., and Kay, L. E. (1997) *J. Mol. Biol. 272*, 790−804.
26. Prompers, J. J., Scheurer, C., and Brüschweiler, R. (2001) *J. Mol. Biol. 305*, 1085−1097.
27. Gagné, S. M., Tsuda, S., Spyracopoulos, L., Kay, L. E., and Sykes, B. D. (1998) *J. Mol. Biol. 278*, 667−686.
28. Spyracopoulos, L., Gagné, S. M., Li, M. X., and Sykes, B. D. (1998) *Biochemistry 37*, 18032−18044.
29. Mandel, A. M., Akke, M., and Palmer, A. G. (1996) *Biochemistry 35*, 16009−16023.
30. Chandra, M., Dong, W.-J., Pan, B.-S., Cheung, H. C., and Solaro, R. J. (1997) *Biochemistry 36*, 13305−13311.
31. Li, M. X., Gagné, S. M., Tsuda, S., Kay, C. M., Smillie, L. B., and Sykes, B. D. (1995) *Biochemistry 34*, 8330−8340.
32. Gagné, S. M., Tsuda, S., Li, M. X., Chandra, M., Smillie, L. B., and Sykes, B. D. (1994) *Protein Sci. 3*, 1961−1974.
33. Golosinska, K., Pearlstone, J. R., Borgford, T., Oikawa, K., Kay, C. M., Carpenter, M. R., and Smillie, L. B. (1991) *J. Biol. Chem. 266*, 15797−15809.
34. Farrow, N. A., Muhandiram, R., Singer, A. U., Pascal, S. M., Kay, C. M., Gish, G., Shoelson, S. E., Pawson, T., Forman-Kay, J. D., and Kay, L. E. (1994) *Biochemistry 33*, 5984−6003.
35. Lavigne, P., Kondejewski, L. H., Jr., Houston, M. E., Jr., Sönnichesen, F. D., Lix, B., Sykes, B. D., Hodges, R. S., and Kay, C. M. (1995) *J. Mol. Biol. 254*, 505−520.
36. Delaglio, F., Grzesiek, S., Vuister, G. W., Zhu, G., Pfeifer, J., and Bax, A. (1995) *J. Biomol. NMR 6*, 277−293.
37. Garrett, D. S., Powers, R., Gronenborn, A. M., and Clore, G. M. (1991) *J. Magn. Reson. 95*, 214−220.
38. Prompers, J. J., and Brüschweiler, R. (2000) *J. Phys. Chem. B 104*, 11416−11424.
39. Schurr, J. M., Babcock, H. P., and Fujimoto, B. S. (1994) *J. Magn. Reson., Ser. B 105*, 211−224.
40. Tjandra, N., Feller, S. E., Pastor, R. W., and Bax, A. (1995) *J. Am. Chem. Soc. 117*, 12562−12566.
41. Luginbühl, P., Pervushin, K. V., Iwai, H., and Wüthrich, K. (1997) *Biochemistry 36*, 7305−7312.
42. Lee, L. K., Rance, M., Chazin, W. J., and Palmer, A. G. (1997) *J. Biomol. NMR 9*, 287−298.
43. Clore, G. M., Szabo, A., Bax, A., Kay, L. E., Driscoll, P. C., and Gronenborn, A. M. (1990) *J. Am. Chem. Soc. 112*, 4989−4991.
44. Evenäs, J., Forsén, S., Malmendal, A., and Akke, M. (1999) *J. Mol. Biol. 289*, 603−617.
45. Seewald, M. J., Pichumani, K., Stowell, C., Tibbals, B. V., Regan, L., and Stone, M. J. (2000) *Protein Sci. 9*, 1177−1193.
46. Wolfram, S. (1996) *The Mathematica Book*, 3rd ed., Cambridge University Press, Cambridge, England.
47. Stone, M. J., Gupta, S., Snyder, N., and Regan, L. (2001) *J. Am. Chem. Soc. 123*, 185−186.
48. Lee, A. L., Kinnear, S. A., and Wand, A. J. (2000) *Nat.Struct. Biol. 7*, 72−77.
49. Hodsdon, M. E., and Cistola, D. P. (1997) *Biochemistry 36*, 2278−2290.
50. Feher, V. A., and Cavanagh, J. (1999) *Nature 400*, 289−293.
51. Crump, M. P., Spyracopoulos, L., Lavigne, P., Kim, K.-Y., Clark-Lewis, I., and Sykes, B. D. (1999) *Protein Sci. 8*, 2041−2054.
52. Mulder, F. A. A., Hon, B., Muhandiram, D. R., Dahlquist, F. W., and Kay, L. E. (2000) *Biochemistry 39*, 12614−12622.
53. Zídek, L., Novotny, M. V., and Stone, M. J. (1999) *Nat. Struct. Biol. 6*, 1118−1121.
54. Abragam, A. (1961) *The principles of nuclear magnetism*, Clarendon Press, Oxford, U.K.
55. Woessner, D. E. (1962) *J. Chem. Phys. 37*, 647−654.
56. Wennerström, H. (1972) *Mol. Phys. 24*, 69−80.
57. Barbato, G., Ikura, M., Kay, L. E., Pastor, R. W., and Bax, A. (1992) *Biochemistry 31*, 5269−5278.

BI010903K